Journal of Materials Chemistry B

ROYAL SOCIETY OF CHEMISTRY

PAPER

View Article Online
View Journal

Cite this: DOI: 10.1039/d0tb01111h

Stabilized albumin coatings on engineered xenografts for attenuation of acute immune and inflammatory responses†

Chao Tao,[a] Wenzhen Zhu,[a] Jabed Iqbal,[b] Chenjie Xu [ac] and Dong-An Wang *[c]

Received 28th April 2020,
Accepted 31st May 2020

DOI: 10.1039/d0tb01111h

rsc.li/materials-b

Xenogeneic grafts are promising candidates for transplantation therapy due to their easily accessible sources. Nevertheless, the immune and inflammatory responses induced by xenografts need to be addressed for clinical use. A novel and facile method was introduced for the attenuation of immune and inflammatory responses by extending the immune evasion potential of albumin to the tissue engineering field and coating albumin, which could passivate biomaterial surfaces, onto xenografts. Albumin was first modified by dopamine to enhance its adhesion on graft surfaces. Porcine chondrocytes derived living hyaline cartilage graft (LhCG) and decellularized LhCG (dLhCG) were applied as xenograft models implanted in the omentum of rats. Both LhCG which contained porcine chondrocytes as well as secreted ECM and dLhCG which was mainly composed of the porcine source ECM showed alleviated immune and inflammatory responses after being coated with albumin at cell, protein and gene levels, respectively. Significantly less inflammatory cells including neutrophils, macrophages and lymphocytes were recruited according to pathological analysis and immunohistochemistry staining with lower gene expression encoding inflammation-related cytokines including MCP-1, IL-6 and IL-1β after employing LhCG and dLhCG with albumin passivation coating.

1. Introduction

Immunocompatibility is a significant issue that should be paid attention to in the tissue engineering field. Xenografts were derived from xenogeneic animals and developed to address the issue of shortage of human-donated organs or other human-source autografts and allografts.[1] Moreover, the fabrication of autografts or allografts might need a pre-surgery on patients which causes pain or damage to patients' tissues or organs. For example, autologous chondrocyte implantation (ACI), a scaffold-based delivery of chondrocytes to cartilage defects involving collecting and implanting autologous chondrocytes, needs two operations and a long recovery time.[2,3] Therefore, xenogeneic sources such as porcine or bovine source grafts are promising candidates for tissue regeneration. However, there are still obstacles that hinder the clinical translation of xenografts. Immune and inflammatory responses elicited in recipients are the most severe issues that need to be addressed.

The immune and inflammatory responses to xenografts were initiated in various ways due to the diverse antigens present in grafts which led to the recognition of foreign bodies by the host. Moreover, novel infectious organisms were possibly transmitted to the recipient and generated more antigens.[4] Since tissue cellular antigenicity is one of the main stimulations of recipient immune responses, decellularization of xenografts has been widely studied as a simple approach toward clinical use. Decellularized porcine cornea,[5,6] decellularized bovine pericardial scaffold[7,8] and other decellularized extracellular matrix (ECM) based grafts[9,10] showed enhanced performance in acceptance by the host immune system compared to fresh xenografts, some of which were even put into clinical trial.[11] However, besides tissue cellular antigenicity, acellular antigens in the ECM, such as α-gal antigen[12] which binds with natural anti-gal antibodies in human, and antigens from homologous proteins[13] of diverse sequences would also contribute to the rejection from recipients and further failure of grafts. Other approaches for the elimination of recipient immune responses included genetic modifications by genome editing tools,[14] glutaraldehyde cross-linking[13] and removal of antigens.[15,16] However, the current existing methods were complicated and might sacrifice ECM constructs, leading to a compromised regenerative effect. In this case, a facile and effective alternative for immune evasion of xenografts such as coating natural biological materials is worth further investigation.

[a] School of Chemical and Biomedical Engineering, Nanyang Technological University, 50 Nanyang Ave, 639798, Singapore
[b] Department of Pathology, Singapore General Hospital, 20 College Road, Academia, Diagnostics Tower, Level 10, Singapore 169856, Singapore
[c] City University of Hong Kong, Tat Chee Avenue, Kowloon, Hong Kong. E-mail: dwang229@cityu.edu.hk

† Electronic supplementary information (ESI) available. See DOI: 10.1039/d0tb01111h

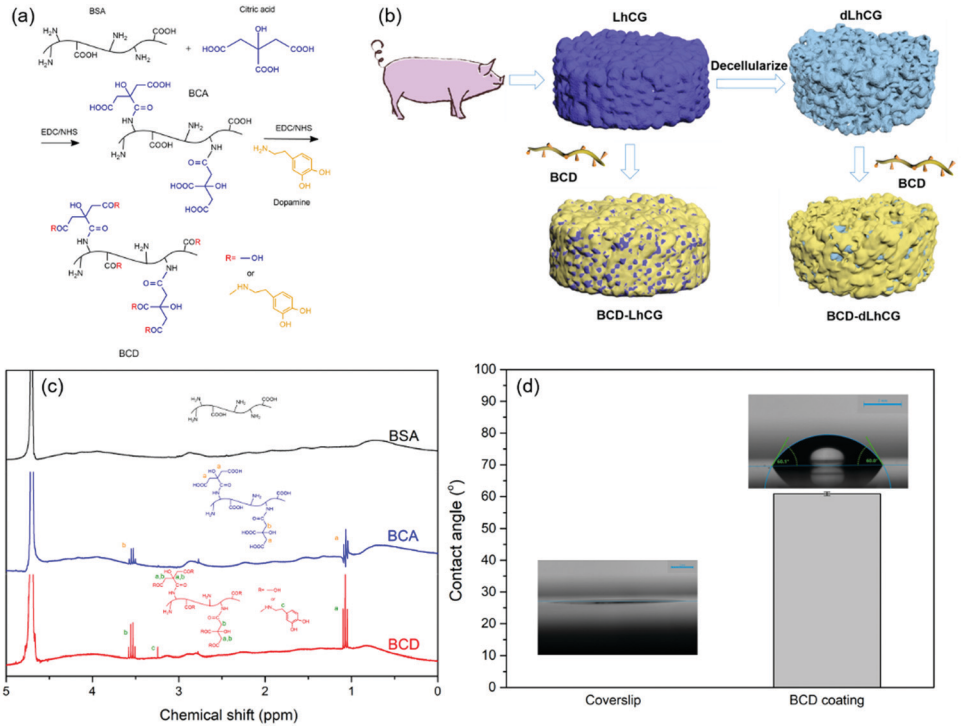

Fig. 1 (a) Preparation of BCD, (b) schematic illustration of BCD-LhCG and BCD-dLhCG, (c) ^{1}H NMR spectra of BSA, BCA and BCD and (d) water contact angles of coverslip with and without BCD coating.

As the most abundant protein and primary vehicle for endogenous compounds in plasma,[17,18] albumin has been widely studied for biomedical applications because it is compatible and commercially available.[19] It is worth noting that albumin is a potent stealth coating for immune evasion since albumin is capable of passivating biomaterial surfaces.[20–22] Albumin on the surface could block other proteins, the absorption of which activates blood coagulation and further inflammation.[23] Albumin has been successfully applied as a camouflage coating on a variety of nanoparticles such as virus-based nanoparticles[24–26] and DNA origami.[27] Endogenous or exogenous albumin has also been either covalently or non-covalently coated on polymers,[28] inorganic nanoparticles[29] and liposomes[30–33] to attenuate immune responses and prolong the blood circulation time. Nowadays, albumin for immune evasion is mainly studied in the drug delivery area on nanoparticles. We herein extended this idea to the tissue engineering field on grafts and developed a facile method for immune evasion of xenografts.

In this study, we took advantage of the non-sticky nature of albumin, transferred it to the tissue engineering field and developed a facile method for evasion from immune rejection elicited by xenografts through coating albumin. The basic idea is to make use of the passivation nature of albumin to avoid adsorption of other proteins and further coagulation. The adhesion of albumin onto grafts was achieved by introducing dopamine, a mussel-inspired adhesive,[34] *via* a chemical reaction which avoids the introduction of free dopamine. Moreover, our group has developed living hyaline cartilage graft (LhCG),[35–38] which is composed of porcine chondrocytes derived ECM with porcine chondrocytes, and decellularized LhCG (dLhCG),[39–41] which is mainly composed of porcine chondrocytes derived ECM, and applied them as xenograft models in this study. This process is briefly illustrated in Fig. 1b. The inflammation process could be divided into acute inflammation, which lasts within a few days to weeks, and chronic inflammation, which is developed from persistent acute inflammation and may last for years.[42,43] We herein focus on studying the attenuation of acute immune and inflammatory responses, the failure of which will lead to severe chronic inflammation and disease. The immunocompatibility of LhCG, dLhCG with and without albumin coatings were evaluated at the cell, protein and gene levels, respectively.

2. Materials and methods

2.1 Materials

Bovine serum albumin (BSA), citrate acid (CA), dopamine hydrochloride, 1-ethyl-3-(3-dimethylaminopropyl)-carbodiimide (EDC), *N*-hydroxysuccinimide (NHS), and sodium hydrate (NaOH) were purchased from Sigma Aldrich for the preparation of dopamine functionalized albumin. Chondrocytes were extracted from the market-available porcine bone for the fabrication of LhCG and dLhCG. Gelatin from bovine skin, alginate acid sodium salt and fluorescein isothiocyanate (FITC) were also purchased from Sigma Aldrich. 1× phosphate buffered saline (1× PBS, pH = 7.4, Gibco) was purchased from Thermo Fisher Scientific. Tris buffer (1.0 M, pH = 8.8) was purchased from 1st Base Pte Ltd, Singapore.

2.2 Preparation of dopamine-functionalized albumin (BCD)

A modified protocol based on EDC/NHS coupling[44] was used for the preparation of the dopamine-functionalized albumin (BCD) coating material. First, 5 mL of CA solution (0.2 g mL^{-1}) with 1× PBS as the solvent was added to a three-neck flask fitted with one N_2 inlet, after which the pH was adjusted to 6.0 by 6 M NaOH solution. Then 0.3 g of EDC and 0.3 g of NHS were added. 1.75 g of BSA was dissolved in 10 mL 1× PBS and added to the flask drop by drop. The mixture reacted for 6 h under 37 °C and pH 5.5–6.0. The products were dialyzed against 1× PBS for 2 days for purification and freeze-dried after that (BT48, Millrock Technology Inc, USA). The resultant purified product was an intermediate product named BCA. Then 1 g of BCA, 1 g of dopamine hydrochloride, 1 g of EDC and 1 g of NHS were dissolved in 100 mL 1× PBS and added to a Schlenk tube. The pH of the mixture was adjusted to around 6.0. Three freeze–thaw cycles were performed to completely remove oxygen to avoid oxidation of dopamine. The mixture reacted under N_2 protection and 37 °C. Finally, the products were dialyzed against 1× PBS for 2 days and freeze-dried to harvest final product BCD. The chemical structures of BCA and BCD were characterized by ^{1}H NMR (Bruker Avance II 300 MHz NMR) with D_2O (Sigma Aldrich, USA) as the solvent.

2.3 Fabrication of LhCG and dLhCG

LhCG[35–38] and dLhCG[39–41] fabricated based on our published protocol were used as model xenografts. Porcine chondrocytes were seeded in alginate hydrogel with gelatin microspheres as micropore forming agent and grown in high glucose Dulbecco's Modified Eagle Medium (DMEM). Chondrocytes grew, proliferated in hydrogels and secreted the extracellular matrix (ECM), forming 3D micro-tissues. After that, the alginate template was removed by rinsing with sodium citrate solution (55 mM in 0.15 M NaCl) to harvest LhCG. Decellularized LhCG by successive physical, chemical and enzymatic methods was named dLhCG.

2.4 Characterization of BCD coating

First of all, in order to prove the feasibility of BCD coating formation, 20 mg mL^{-1} of BCD in Tris buffer (10 mM, pH 8.5) was coated onto the surface of coverslip (CellPath Ltd, UK) by drip coating and drying under room temperature overnight. The water contact angle was detected on a Kruss DSA25 Contact Angle Analyzer with a 5 μL deionized (DI) water drop. The final contact angle result was averaged from five samples' values.

dLhCG and LhCG were rinsed in 20 mg mL^{-1} BCD overnight with Tris buffer (10 mM, pH 8.5) and culture medium as the solvent, respectively, to obtain BCD coated dLhCG (BCD-dLhCG) and BCD coated LhCG (BCD-LhCG). DI water and pure culture medium were applied after that respectively to wash BCD-dLhCG and BCD-LhCG. For visualization of BCD coating on grafts, BCD was labeled with FITC (BCD-FITC) through chemical reactions. Briefly, the isothiocyanate group on FITC reacted with amino groups on BCA (BCA-FITC), after which the BCA-FITC went through an EDC/NHS coupling with dopamine hydrochloride according to the protocol mentioned above. A UV-vis spectrometer (UV-2450, Thermo Fisher USA) was used to ensure the successful conjugation and estimate the fluorophore to protein ratio (F/P) for BCA-FITC and BCD-FITC according to a reported equation:[45]

$$\frac{F}{P} = \frac{A_{max} \times \varepsilon_{prot}}{(A_{280} - cA_{max}) \times \varepsilon_{dye}} \quad (1)$$

where A_{max} is the absorbance value at around 500 nm in this study; A_{280} is the absorbance value of albumin at around 280; c is the correction factor for adjustment of absorption at 280 nm contributed by FITC (c = 0.29 referring to ref. 45); ε_{prot} (ε_{prot} = 43 645 M^{-1} cm^{-1} referring to ref. 46) is the molar extinction coefficient for bovine serum albumin in this study and estimated from amino acid sequence; ε_{dye} (ε_{dye} = 63 096 M^{-1} cm^{-1} referring to ref. 45) is the molar extinction coefficient of FITC in this study.

BCD-FITC was subsequently coated onto dLhCG and LhCG based on the above-mentioned methods, then fixed in 4% paraformaldehyde (Sigma Aldrich, USA), embedded in paraffin (Surgipath® Paraplast®, Leica, USA), sectioned on a slicer (RM2255, Leica, USA) and observed under a fluorescence microscope (Olympus IX71S1F-3, Japan).

The surface elemental information about carbon (C), oxygen (O), nitrogen (N), phosphorous (P) and sulfur (S) was investigated by X-ray photoelectron spectroscopy (XPS) on a Kratos AXIS Supra spectrometer with a 40 eV bandpass energy. The high-resolution C spectra were fitted using Origin 9.0. Before XPS measurements, dLhCG and BCD-dLhCG were freeze-dried, while LhCG and BCD-LhCG were dried in a critical point dryer (CPD) (K850, Quorum Technologies Inc., England) after fixation by 2.5 v/v% glutaraldehyde (Sigma Aldrich, USA) and gradient dehydration in ethanol.

The stability of BCD coating on LhCG and dLhCG was measured by using a BCG Albumin Assay Kit (Sigma Aldrich, USA) *via* testing the BCD content on per milligram dried graft. BCD-dLhCG was digested by collagen II solution after rinsing with DI water for 1 day, 7 days, 14 days and 21 days, respectively. BCD-LhCG went through freeze–thaw cycles three times, followed by being digested in collagen II solution. The BCD content in the digested samples was tested. dLhCG and LhCG were also digested following the same protocol and tested by using the same assay kit at corresponding time points as background.

2.5 Morphology of BCD-LhCG and BCD-dLhCG

The morphology of dLhCG, BCD-dLhCG, LhCG and BCD-LhCG was observed by using a scanning electron microscope (SEM) (JEOL JSM 6700F, Japan). dLhCG and BCD-dLhCG were dried in a freeze dryer, while LhCG and BCD-LhCG were dried in the CPD as mentioned above. Platinum was coated onto the samples by sputtering for 120 s (JFC-1600, JEOL Asia Pte. Ltd, Japan) before SEM observation.

2.6 Cytotoxicity of dLhCG and BCD-dLhCG

Before implanted *in vivo*, the cytotoxicity of BCD-dLhCG and dLhCG was measured by using a WST-1 Assay Kit (Sigma Aldrich, USA). Chondrocytes were cultured in wells of 96 well

plate (2500 cells per well) and incubated with dLhCG and BCD-dLhCG respectively for 1 days, 4 days and 7 days. The culture medium at certain time points was collected and incubated together with WST-1 for 3 h. The detection and calculation were carried out according to the manufacturer's protocol.

2.7 *In vivo* immunocompatibility study in a rat omentum implantation model

All animal experiment protocols have been approved by Institutional Animal Care and Use Committee (IACUC), Nanyang Technological University, Singapore according to the local law.

A rat omentum implantation model was applied to study *in vivo* immune and inflammatory performance of LhCG, BCD-LhCG, dLhCG and BCD-dLhCG. Forty-eight Sprague Dawley female rats (n = 4, 250–300 g) were divided into six groups. Besides the four groups mentioned above, natural porcine cartilage discs with a diameter of $\sim$0.5 cm were decellularized following the same protocol as LhCG was decellularized and chosen as a positive control. Natural autologous cartilage slices were collected from rat ears of the negative control group and implanted into the omentum of the same individual. First, an incision of around 2 cm was cut on the rats' abdomen. Each rat was embedded with two grafts ($\sim$0.5 cm in diameter) of the same group, after which the incision was closed by 4–0 Nylon sutures and stainless-steel clips. Two time points, day 1 and day 14, were chosen for the collection and characterization of grafts. Specifically, the implanted two grafts and surrounding tissues were collected from the omentum, one of which was fixed in 4% paraformaldehyde for staining, the other was kept in 1× PBS for gene expression evaluation.

2.7.1 Pathological analysis. A pathologist who was blinded to the experimental groups carried out the pathological analysis by evaluating the infiltrated inflammatory cell conditions according to a five-point grading scheme[47–50] based on hematoxylin and eosin (H&E) (Sigma Aldrich, USA) staining results. The grafts and surrounding tissues were fixed in 4% paraformaldehyde, embedded, sectioned and stained with H&E following a standard protocol from the manufacturer.

2.7.2 Immunohistochemistry analysis. The sectioned samples were stained with MPO (Myeloperoxidase), CD68 and CD3 for the detection of neutrophils, macrophages and T cells, respectively, by immunohistochemistry (IHC) staining with an UltraVision™ Quanto Detection System HRP DAB kit (Thermo Fisher Scientific, UK). The details of antibodies are listed as follows: Anti-MPO (Abcam, ab9535), Anti-CD68 (Abcam, ab31630) and Anti-CD3 (Abcam, ab16669).

2.7.3 Gene expression. The gene expression of inflammation related cytokines including monocyte chemoattractant protein-1 (MCP-1), interleukin-6 (IL-6) and interleukin-1β (IL-1β) was quantified by quantitative real-time polymerase chain reactions (qRT-PCR) and semi-quantified by agarose gel electrophoresis.

First of all, total RNA was extracted by using a TRIzol® reagent (Life Technology, USA), after which the RNA concentration was detected by using a NanoDrop 2000c (Thermo Fisher Scientific, USA). Then cDNA was synthesized and reverse transcription was performed with reagents purchased from Promega. qRT-PCR was carried out on a CFX Connect Real-Time PCR System (BIO-RAD, USA). Primers, purchased from Integrated DNA Technologies Singapore, are listed in Table S1 (ESI†). GAPDH gene was used as a housekeeping gene for normalization of target genes. A comparative $2^{-\Delta\Delta C_T}$ method was applied for the calculation.

Furthermore, cDNA was amplified with Taq DNA polymerase (NEW ENGLAND BioLabs, England) and visualized by agarose gel electrophoresis in Tris–Borate–EDTA buffer (Vivantis Technologies, Malaysia) after mixing with SYBR® Safe DNA gel stain (Invitrogen, USA).

3. Results

3.1 Characterization of BCD macromolecules and BCD coating

The preparation of BCD is illustrated in Fig. 1a. First of all, the BCA prepolymer was prepared by grafting CA onto BSA through EDC/NHS coupling for the introduction of extra carboxyl for additional reaction sites. After that, dopamine was grafted onto BCA by EDC/NHS coupling to synthesize BCD, so that no free dopamine will be introduced.

The chemical structures of BCA and BCD were characterized by ^{1}H NMR and are shown in Fig. 1c. Peaks at around 3.5 ppm and 1.1 ppm on the ^{1}H NMR spectrum of BCA belong to –COC$\underline{H}_2$– and –C$\underline{H}_2$COOH respectively on the grafted citric acid, confirming the successful modification by citric acid. Moreover, the appearance of the signal at around 3.2 ppm on the ^{1}H NMR spectrum of BCD belonged to –NH–CH$_2$–C$\underline{H}_2$– on grafted dopamine and confirmed the successful introduction of dopamine.

BCD was first coated onto the coverslip to evaluate its coating formation feasibility and wettability. Water contact angles of the coverslip surface with and without BCD coating were measured. It is shown in Fig. 1d that the water contact angle increased to 60.9° ± 0.6° from around 0°, indicating the formation of a uniform BCD coating on the superhydrophilic coverslip surface. After that, BCD was coated onto LhCG and dLhCG for further investigation, the schematic illustration of which is shown in Fig. 1b.

3.2 Characterization of BCD coating on grafts

In order to visualize BCD coating on grafts, FITC was grafted onto BCD for labeling (Fig. 2a). The absorbance peak at around 500 nm on the UV-vis spectrum belongs to BCA-FITC, while that at around 277 nm belongs to unlabeled BCA (Fig. 2b). Similarly, two absorbance peaks at 287 nm and 507 nm shown in Fig. 2c belong to unlabeled BCD and BCD-FITC, respectively. The presence of an absorbance peak at around 507 nm confirmed the existence of BCD-FITC. The F/P ratio of BCA-FITC ($\sim$2.2) and BCD-FITC ($\sim$1.5) was estimated based on eqn (1).

Subsequently BCD-FITC was coated onto dLhCG and LhCG and observed under a fluorescence microscope. BCD was mainly uniformly coated on the surface of the whole dLhCG graft (Fig. 2d) and preferred to adhere to the cell membrane compared

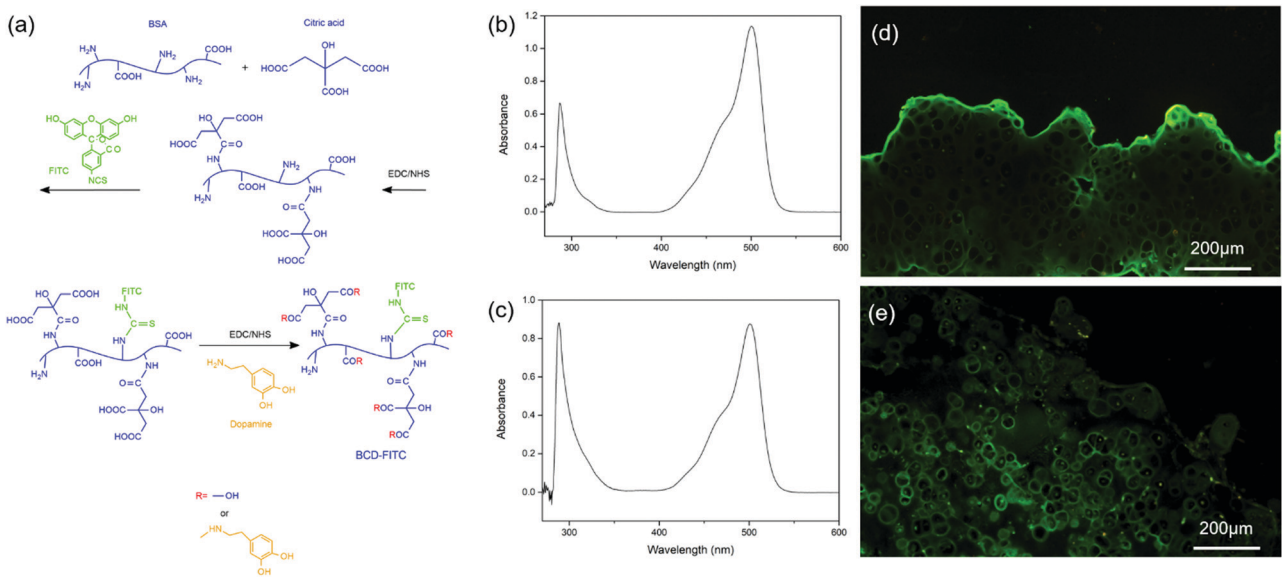

Fig. 2 (a) Preparation of BCD-FITC, UV-vis spectrum of (b) BCA-FITC and (c) BCD-FITC, fluorescent image of (d) BCD-dLhCG and (e) BCD-LhCG.

Table 1 Surface elemental composition of dLhCG, BCD-dLhCG, LhCG and BCD-LhCG[a]

	C (%)							
	C–C/ C–H	C–N/C–S/ C–O	C═O	–O–C═O	O (%)	N (%)	P (%)	S (%)
dLhCG	18.0	13.1	5.1	2.6	36.5	20.3	1.3	3.1
BCD-dLhCG	15.4	12.6	5.9	2.8	34.8	23.1	1.3	4.1
LhCG	19.4	11.5	8.4	0.8	29.7	23.0	3.8	3.4
BCD-LhCG	17.6	13.1	6.9	2.5	29.4	23.9	1.9	4.7

to ECM on LhCG (Fig. 2e). XPS was conducted to further detect the chemical information on graft surfaces within 10 nm. Albumin was rich in cysteine (Cys), which could not be detected in collagen. In this case, albumin was more abundant in S than collagen. According to Table 1, the S content of dLhCG increased from 3.1% to 4.1% after being coated with BCD, confirming the successful coating of BCD onto dLhCG. Similarly, there was an increase in the S content of BCD-LhCG (4.7%) compared to LhCG (3.4%), confirming the successful coating of BCD onto LhCG. dLhCG was decellularized and rarely contained phosphorus which was one of the main elements constituting the cell membrane. Therefore, LhCG (3.8%) contained more P compared to dLhCG (1.3%). However, due to the existence of BCD coating on the surface, there was not much difference in the P content of BCD-dLhCG (1.3%), and BCD-LhCG (1.9%) compared to dLhCG (1.3%). Moreover, the P signal at around 132 eV was nearly invisible in the XPS spectrum of BCD-dLhCG (Fig. 3a). Besides, the high resolution C 1s spectra were fitted with peaks at around 284.7 eV (C–C, C–H), 286.1 eV (C–N, C–S, C–O), 287.8 eV (C═O) and 288.5 eV (–O–C═O) and shown in Fig. 3b–e.

3.3 Stability of BCD coating on grafts

The stability of BCD coating should be taken into consideration to ensure the existence of disguise coating before cells migrate in and proliferate. Bromocresol green could specifically bind with albumin and form a colored complex whose intensity at 620 nm is proportional to albumin concentration. Durability was measured based on this reaction by using a BCG Albumin Assay Kit. As shown in Fig. 4a and b, the BCD content decreased on day 7 compared to day 1 result, but remained almost the same from the 7th day on.

3.4 Morphology of grafts

The morphology of dLhCG, BCD-dLhCG, LhCG and BCD-LhCG was observed under the SEM. As shown in Fig. 4c, there was a porous structure observed in dLhCG with the pore size in tens of microns. The BCD coating did not damage the porous structure of dLhCG and was visible under the SEM (Fig. 4e). Abundant assembled chondrocytes could be observed in LhCG and BCD-LhCG under the SEM (Fig. 4d and f). Therefore, LhCG with and without BCD coating was more densely packed compared to dLhCG and BCD-dLhCG.

3.5 *In vivo* rat omentum implantation for evaluation of immunocompatibility

Before *in vivo* implantation, the cytotoxicity of dLhCG and BCD-dLhCG was evaluated on chondrocytes by WST-1. dLhCG and BCD-dLhCG showed no cytotoxicity with cell viabilities of 89.4% ± 2.7% and 92.5% ± 14.2% after 7 days of incubation, respectively (Fig. S1, ESI†). And BCD coating did not interfere with the biocompatibility of dLhCG and showed comparable cell viability on day 1, day 4 and day 7.

Embedded grafts and surrounding tissues were collected on day 1 and day 14 for the evaluation of acute immune and inflammatory responses. Photographs of the collected grafts are shown in Fig. 5a. Obvious blood coagulation was observed surrounding the LhCG graft collected on day 14, indicating a possible severe inflammation. Pathological analysis, IHC staining and PCR were further carried out for assessment at the cell level, protein level and gene level, respectively. First of

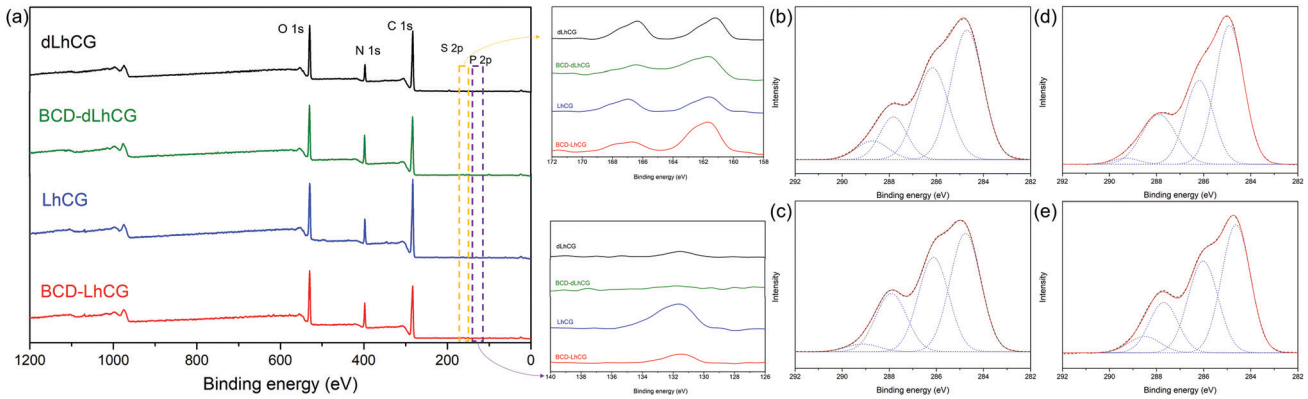

Fig. 3 (a) XPS spectra of dLhCG, BCD-dLhCG, LhCG and BCD-LhCG, P 2p and S 2p spectra were zoomed in and shown aside, XPS spectrum of C 1s for (b) dLhCG, (c) BCD-dLhCG, (d) LhCG and (e) BCD-LhCG.

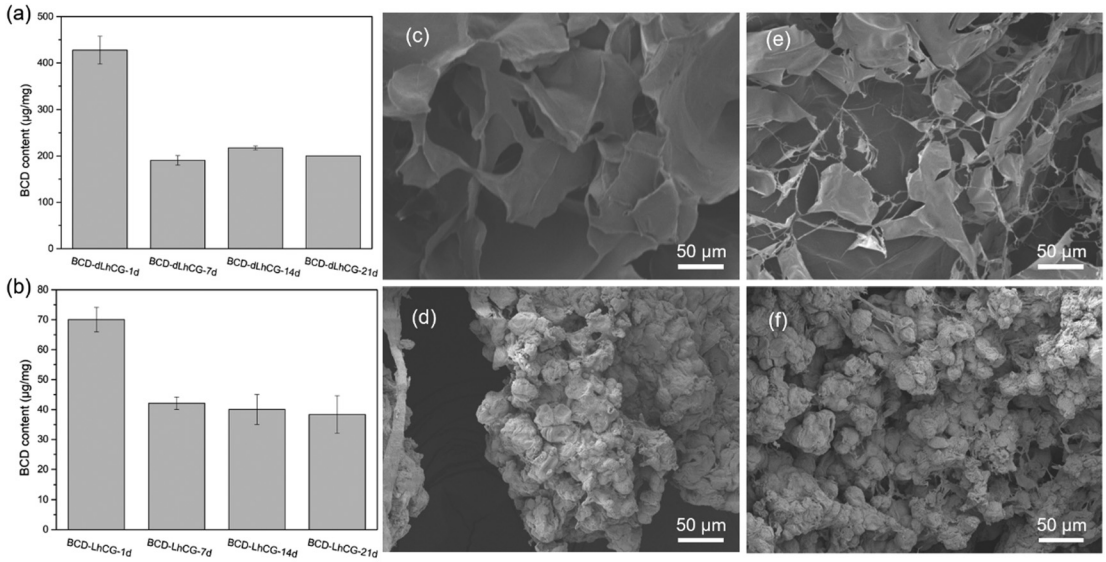

Fig. 4 BCD content of (a) BCD-dLhCG and (b) BCD-LhCG after rinsing in DI water for 1 days, 7 days, 14 days and 21 days, respectively, and SEM images of (c) dLhCG, (d) LhCG, (e) BCD-dLhCG and (f) BCD-LhCG.

all, there were no hyperacute immune and inflammatory responses with all rats surviving.

3.5.1 Pathological analysis. Three kinds of inflammatory cells including neutrophils which are characterized by multi-lobed nucleus, macrophages which are characterized by small oval or indented nuclei with relatively luxuriant cytoplasm and lymphocytes which are characterized by round dark nuclei with relative scarce cytoplasm were quantified by a pathologist who was blinded to the experimental design and groups and are plotted in Fig. 5b–d according to a five-point grading scheme, where no inflammatory cells showing in any field scored 0, scattered sparse inflammatory cells showing in the high power field scored 1, inflammatory cells showing in at least one low power field scored 2, abundant inflammatory cells showing in every low power field scored 3, and bad inflammatory cell infiltration visible in the low power field scored 4 (Fig. 5e).

Neutrophils were the first inflammatory cells to migrate out of the blood stream to the inflammation site. As shown in Fig. 5b, on day 1 post-surgery, there showed the most serious neutrophil infiltration in LhCG and dLhCG, followed by PC which was mild in neutrophil infiltration. Minimal to mild neutrophil infiltration was observed in BCD-LhCG. By contrast, there were minimal neutrophils in BCD-dLhCG and negative control RE. As the first inflammatory cells migrating in, neutrophils had a short lifespan. As a result, 14 days later, there showed few neutrophils in all grafts. Macrophages and lymphocytes were later introduced into the implantation site. According to Fig. 5c, on day 1 post-surgery, moderate macrophages were present in LhCG, which showed the most severe macrophages infiltration among all grafts. PC came next with mild to moderate macrophage infiltration. Mild macrophages were observed in dLhCG. Minimal to mild macrophages could still be detected in BCD-LhCG, while macrophage infiltration was nearly negligible in BCD-dLhCG as well as RE. On day 14 post-implantation, macrophage infiltration levels almost remained as it was on day 1 except for a more intensively macrophage

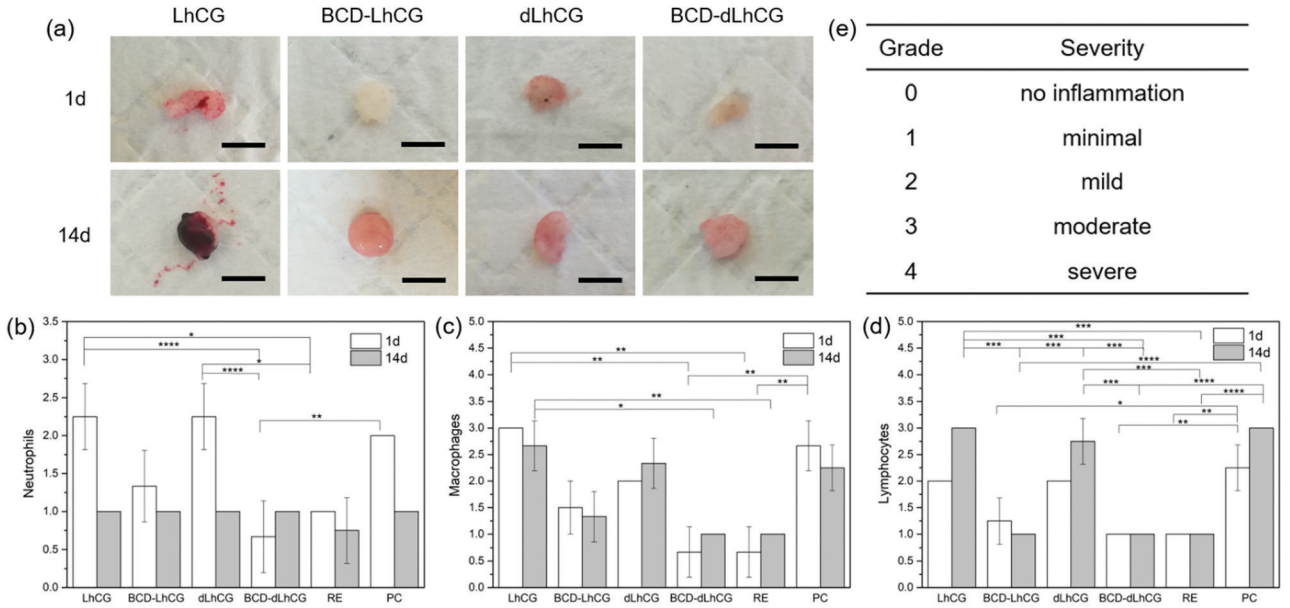

Fig. 5 (a) Photographs of samples collected from sacrificed rats, scale bar = 0.5 cm, pathological analysis based on quantitative assessment of inflammatory cells including (b) neutrophils, (c) macrophages, (d) lymphocytes on day 1 and day 14 based on (e) the 5-point grading system (*$p < 0.05$, **$p < 0.01$, ***$p < 0.001$, ****$p < 0.0001$) ($n = 4$ for every group).

invasion ranging from mild to moderate observed in dLhCG. As shown in Fig. 5d, on day 1 post-implantation, lymphocyte infiltration was not severe in all grafts with mild infiltration in PC, dLhCG and LhCG, minimal to mild in BCD-LhCG and minimal in BCD-dLhCG and RE. 14 days later, LhCG, PC and dLhCG were moderately infiltrated by lymphocytes, while that in BCD-LhCG, BCD-dLhCG and RE remained minimal.

3.5.2 IHC staining. IHC staining of MPO, CD68 and CD3 was conducted for identification of neutrophils, macrophages and T cells respectively, to determine their location, and to evaluate their immune and inflammatory responses at a protein level. IHC staining images for LhCG, BCD-LhCG, dLhCG and BCD-dLhCG are shown in Fig. 6, and those of positive control PC (Fig. S2, ESI†) as well as negative control RE (Fig. S3, ESI†) are provided in the ESI.† On day 1 post-implantation (Fig. 6a), MPO, a peroxidase enzyme abundantly expressed in neutrophils, was mainly distributed on the surface of LhCG with some inside LhCG. Abundant MPO was observed all over the whole dLhCG graft. By comparison, only minimal MPO was found on the surface of BCD-LhCG and nearly no MPO was stained in BCD-dLhCG. CD68 is expressed in macrophages. CD68 was mainly found on the surface of LhCG and all over dLhCG. Sparse CD68 could be observed in BCD-LhCG, while only minimal CD68 was detected near the surface of BCD-dLhCG. CD3 is a symbol for T cells. There was CD3 distributed both on the surface and inside LhCG. CD3 was also observed inside dLhCG. CD3 was present on the surface of BCD-LhCG. And only minimal CD3 was sparsely present in BCD-dLhCG. On day 14 post-implantation (Fig. 6b), MPO could still be found in some areas of LhCG and dLhCG, while no obvious MPO was detected in BCD-LhCG and BCD-dLhCG. CD68 was intensively distributed in LhCG and uniformly distributed in dLhCG. Nearly no CD68 was present in BCD-LhCG and BCD-dLhCG. Moreover, intensive stained CD3 could be observed inside LhCG and dLhCG. By contrast, CD3 was nearly invisible in BCD-LhCG and BCD-dLhCG.

3.5.3 PCR. qRT-PCR and agarose gel electrophoresis were carried out for the evaluation of inflammatory and immune responses quantitatively and qualitatively at a gene level. Expression of inflammation-related genes involving MCP-1, IL-6 and IL-1β was measured. On day 1 post-implantation, as shown in Fig. 7a, LhCG expressed the most MCP-1, followed by PC and dLhCG. MCP-1 expression was still detectable in BCD-LhCG and slightly visible on agarose gel. MCP-1 was negligible in BCD-dLhCG and RE. IL-6 showed the highest expression in PC, followed by dLhCG. There was also an obvious IL-6 expression detected in LhCG (Fig. 7b). PC showed the highest value in IL-1β expression, followed by dLhCG and LhCG. And IL-1β expression was nearly invisible in BCD-LhCG, BCD-dLhCG and RE on agarose gel (Fig. 7c). On day 14 post-implantation, dLhCG showed the highest MCP-1 expression, followed by LhCG. MCP-1 expression in PC was relatively lower than LhCG and dLhCG but still obvious. By contrast, nearly no MCP-1 was detected in BCD-LhCG, BCD-dLhCG or RE (Fig. 7e). IL-6 expression could be detected in LhCG, dLhCG and PC, while that in BCD-LhCG, RE and BCD-dLhCG was invisible (Fig. 7h) with a low expression value (Fig. 7f). As for IL-1β (Fig. 7g), LhCG showed the highest expression value with PC and dLhCG followed. Moreover, there was slight IL-1β expressed in BCD-LhCG which was confirmed on agarose gel. However, IL-1β expression in RE and BCD-dLhCG was not detected.

4. Discussion

In this study, a facile approach for the attenuation of inflammatory and immune responses of xenografts by coating albumin on the

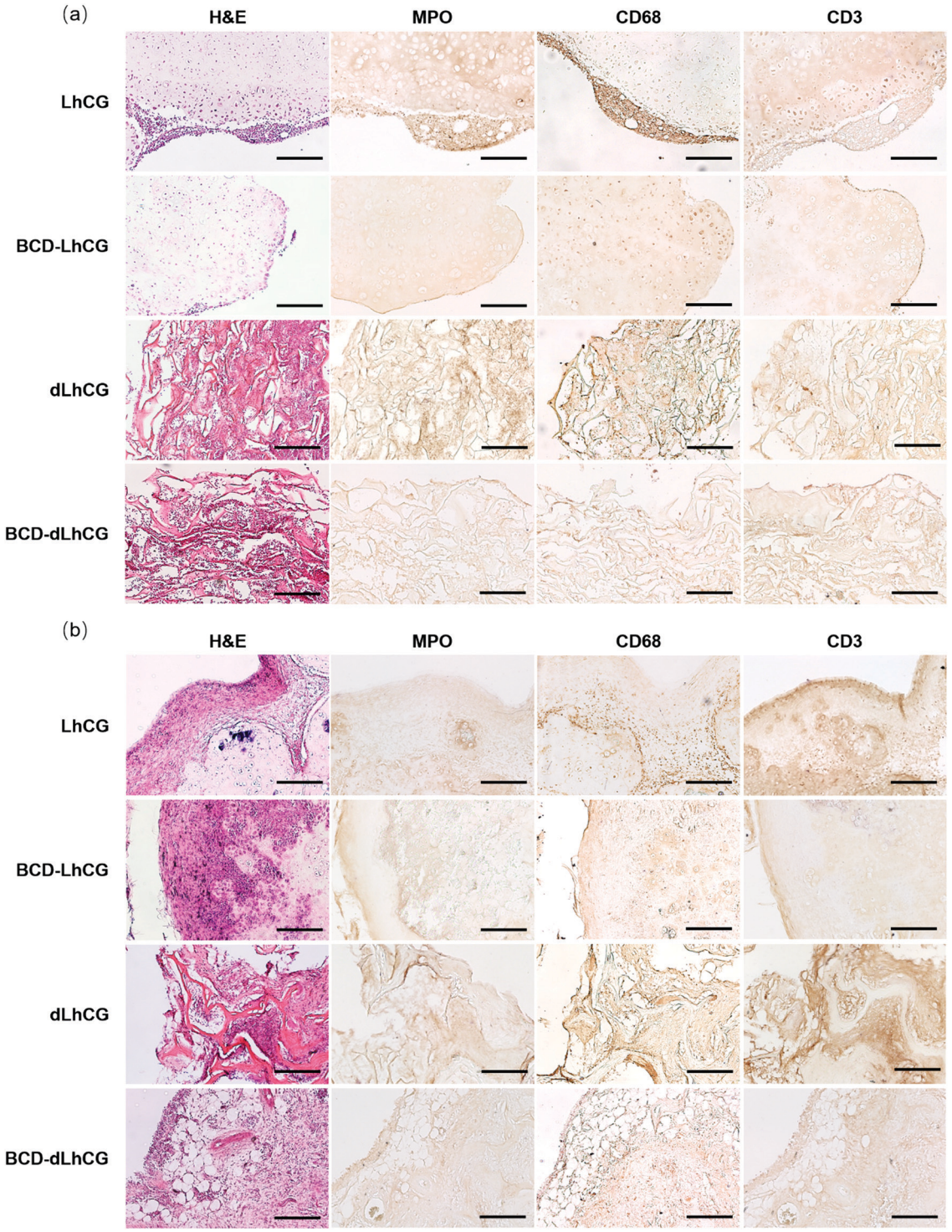

Fig. 6 H&E and IHC staining images for (a) day 1 and (b) day 14 grafts, scale bar = 200 μm.

surface was introduced. LhCG and dLhCG which were derived from the porcine source ECM based on our previously published protocol were chosen as the model xenografts. First of all, in order to improve the adhesion of albumin on xenografts, albumin was modified by dopamine, a mussel-inspired adhesive *via* EDC/NHS coupling (Fig. 1a). The chemical structures of intermediate product BCA and final product BCD were determined by ^{1}H NMR (Fig. 1c). The appearance of signals at 3.5 ppm of –COC$\underline{H}_2$– and 1.1 ppm of –C$\underline{H}_2$COOH confirmed the successful introduction of citric acid onto BSA. Moreover, the appearance of signal at 3.2 ppm of –NH–CH$_2$–C$\underline{H}_2$– confirmed the successful modification of BCA by dopamine. Subsequently, the feasibility of BCD coating formation was tested on a coverslip and confirmed with an increase in the water contact angle

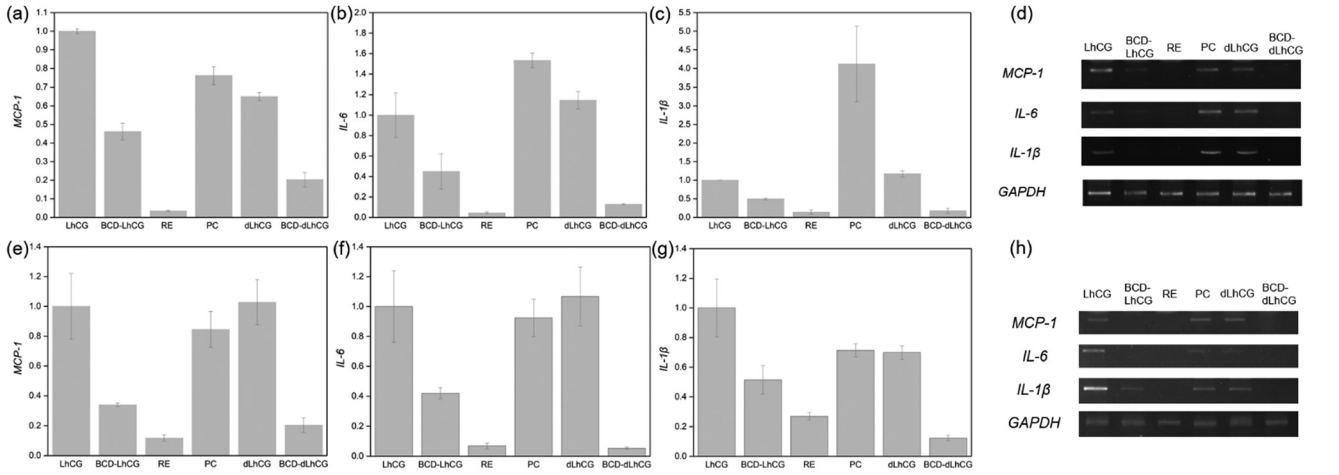

Fig. 7 Gene expression of (a) MCP-1, (b) IL-6, (c) IL-1β for day 1 grafts and (e) MCP-1, (f) IL-6, (g) IL-1β for day 14 grafts, and gel electrophoresis of GAPDH, MCP-1, IL-6 and IL-1β for (d) day 1 grafts and (h) day 14 grafts.

of the coverslip surface from 0° to 60.9° ± 0.6° after being coated with BCD (Fig. 1d).

Characterization of BCD coating on grafts was conducted by fluorescent microscopy and XPS. First of all, BCD was labeled with FITC by chemical reaction. Briefly, the isothiocyanate group on FITC reacted with amino groups on BCA to obtain intermediate polymer BCA-FITC. Then BCD-FITC was synthesized through an EDC/NHS coupling between BCA-FITC and dopamine (Fig. 2a). The successful labeling was confirmed by using a UV-vis spectrometer. The absorption at around 280 nm and 500 nm belong to the absorption of protein and bound FITC, respectively. The ratio of fluorescein to final protein product (F/P) could be estimated by measuring absorbance at the two wavelengths. The F/P ratio is determined as the moles of FITC to moles of protein. The F/P ratios of BCA-FITC and BCD-FITC were 2.2 and 1.5 respectively and calculated based on absorbance at around 280 nm and 500 nm (Fig. 2b and c) according to eqn (1). BCD-FITC was further coated onto dLhCG and LhCG, after which the samples were sectioned and observed under a fluorescence microscope. As shown in the fluorescent images, BCD was uniformly coated onto the surface of dLhCG (Fig. 2d), while BCD was inclined to adhere to the cell membrane of chondrocytes in LhCG (Fig. 2e). The preference of BCD to the cell surface compared to the matrix surface in LhCG was probably caused by the mobility of the cell membrane. BCD was attached to the cell membrane while moving along with the cell membrane flow. Furthermore, XPS was carried out for analysis of surface chemistry. dLhCG and LhCG are porcine derived ECM based grafts, containing mainly collagen and glycosaminoglycan.[35,40] Collagen has abundant glycine residues which account for about 1/3 and proline residues but no tryptophan or cysteine,[51] while albumin is relatively rich in cysteine.[52] In this case, albumin has more sulphur compared to collagen. According to Table 1, the sulphur content of the dLhCG surface increased to 4.1% from 3.1% after being coated with BCD, while that of the LhCG surface increased to 4.7% from 3.4% after being coated with BCD, indicating the successful coating of BCD onto the graft surface. In addition, it is worth noting that phosphorus accounted for 1.9% on the BCD-LhCG surface, much lower than that on the LhCG surface (3.8%) and comparative to that of dLhCG (1.3%) and BCD-dLhCG (1.3%). dLhCG is constituted mainly by collagen and glycosaminoglycan. BCD is a dopamine modified albumin. The cell membrane has a phospholipid bilayer structure. In this case, the cell membrane was the primary source of phosphorus, contributing to the higher phosphorus content in LhCG than dLhCG and BCD-dLhCG. What is more, the lower phosphorus content on the BCD-LhCG surface than the LhCG surface was in accordance with the fluorescence microscopy result that BCD was inclined to adhere to the cell membrane in LhCG (Fig. 2e).

Only when the BCD coating survives at least until cells migrate in and proliferate, the BCD coating will work for immune evasion. In this case, the durability of BCD coating on xenografts should be paid attention. As shown in Fig. 4a and b, there was a decrease of BCD content on day 7, which might be caused by the removal of the nonspecific absorption of BCD on dLhCG and LhCG. However, after day 7, the BCD content on both LhCG and dLhCG became quite stable with no obvious decrease observed as time went by. The BCD coating was stable for at least 21 days on dLhCG and LhCG, which guaranteed its use as a disguise for alleviation of acute immune and inflammatory responses.

The morphologies of dLhCG, BCD-dLhCG, LhCG and BCD-LhCG were measured under the SEM. A porous structure was observed in dLhCG (Fig. 4c), while chondrocytes assembled in a dried LhCG graft, resulting in a relatively densely packed structure compared to dLhCG (Fig. 4d). BCD-dLhCG kept the porous structure with BCD visible on the surface (Fig. 4e). It is reported that physical properties like pore size[53] or stiffness[54] could affect the immune and inflammatory behavior and resolution. The pore sizes of dLhCG and BCD-dLhCG are in tens of microns which are large enough for inflammatory cells to pass and infiltrate. Therefore, the effect of pore size herein on immune and inflammatory responses could be eliminated. Similar to LhCG, the clusters of chondrocytes were observed in BCD-LhCG (Fig. 4f).

After characterization of BCD coating on grafts *in vitro*, *in vivo* evaluation of inflammatory and immune responses were measured in a rat omentum implantation model. Great omentum refers to layers of apron-like peritomeum surrounding abdominal organs, which are sensitive to foreign bodies. It will be more evident for the grafts not to elicit inflammatory and immune responses if they survive in omentum. First of all, a cytotoxicity test was conducted on dLhCG and BCD-dLhCG before they were embedded into omentum. As shown in Fig. S1 (ESI†), there was a slight decrease in cell viability as time went by but still over 85% chondrocytes were viable in both groups on day 7. And there was no obvious difference in cell viability between the dLhCG group and BCD-dLhCG group.

First of all, no hyperacute immune response occurred with all rats alive. And it is worth noting that the LhCG graft collected on day 14 was covered by blood coagulation, implying a possible severe inflammation (Fig. 5a). Then pathological analysis, IHC staining and PCR were applied for a further assessment of inflammatory and immune responses at the cell, protein and gene levels respectively.

Immune and inflammatory responses are highly coordinated processes involving inflammatory cells. Neutrophils are the first white blood cells to respond to inflammation activated by foreign bodies, release factors to attract monocytes and present antigens to activate T cells.[55] Macrophages mainly carry out phagocytosis and produce growth factors and cytokines such as some pro-inflammatory cytokines like IL-6 and IL-1β.[56] T cells are activated by antigen-receptor ligation as well as signals from antigen-presenting cells and introduced mainly to destroy cells which have been infected with antigens from transplanted foreign bodies. Performances on acute immune and inflammatory responses were evaluated in this study on day 1 and day 14 since acute immune and inflammatory responses reacted and deteriorated rapidly and would progress into persistent chronic responses.[42]

On day 1 post-implantation, LhCG induced the most severe immune and inflammatory responses that were comparable to that of the positive control PC. LhCG showed mild to moderate neutrophil infiltration (Fig. 5b) observed mainly on the surface of LhCG and surrounding tissues (Fig. 6a), moderate macrophage infiltration (Fig. 5c) with macrophages intensively distributed in the surrounding tissues and sparsely distributed inside graft (Fig. 6a), and mild lymphocyte infiltration (Fig. 5d) with T cells distributed intensely on the surface of LhCG and sparsely distributed inside the graft (Fig. 6a). There was an obvious inflammation induced by dLhCG. dLhCG was infiltrated mildly by macrophages and lymphocytes and more seriously by neutrophils (Fig. 5), indicating dLhCG was undergoing an early phase of acute immune and inflammatory responses. Moreover, inflammatory cells were found all over the dLhCG graft, especially neutrophils and macrophages (Fig. 6a). Both LhCG and dLhCG elicit relatively severe immune and inflammatory responses because of their xenogeneic source proteins in the ECM. The more serious inflammation in LhCG than dLhCG was possibly due to the extra antigens present on porcine chondrocytes in LhCG leading to the recognition of foreign bodies. Furthermore, inflammatory cells were observed mainly on the surface of LhCG and its surrounding tissues, while inflammatory cells infiltrated in dLhCG were distributed mainly inside the graft. It is because the porous structure, which was confirmed by SEM (Fig. 4c), provided dLhCG with a larger contact surface area with tissues and more space for cells to migrate in. By contrast, inflammation in the relatively densely packed LhCG was observed mostly on the surface and surrounding tissues on day 1 post-implantation. However, immune and inflammatory responses were alleviated after coating xenografts with BCD. There were minimal to mild neutrophils and lymphocytes observed only on the surface and a few macrophages were found inside BCD-LhCG. The slight inflammation in BCD-LhCG was probably caused by part of the antigens in the ECM being exposed. According to *in vitro* fluorescent images (Fig. 2e), there was a preference of BCD coating to adhere to cell membranes, causing some part of the ECM exposed to tissues. Moreover, there was nearly no inflammation in BCD-dLhCG with minimal inflammatory cells infiltrated which was comparative to the performance of negative control RE.

On day 14 post-implantation, as the first inflammatory cells to migrate in with short lifespan, number of infiltrated neutrophils reduced to minimal in all grafts. LhCG exhibited the most serious inflammation with mild to moderate macrophages infiltrated in LhCG (Fig. 5c) especially at the interface of graft and surrounding tissues (Fig. 6b), and moderate lymphocytes infiltrated (Fig. 5d) both inside graft and on the surface of surrounding tissues (Fig. 6b). dLhCG also induced obvious immune and inflammatory responses which were comparative to that of positive control PC. Mild to moderate macrophage and lymphocyte infiltration (Fig. 5c and d) were observed inside dLhCG (Fig. 6b). What is more, BCD was proved to work as a stealth coating for xenografts to evade from immune recognition with inflammatory cells nearly invisible in BCD-LhCG and BCD-dLhCG grafts.

Immune and inflammatory responses at a gene level were evaluated followed by evaluation at cell and protein levels. Inflammation related gene expressions including MCP-1, IL-6 and IL-1β were measured. Inflammation related cytokines including MCP-1, IL-6 and IL-1β are another significant indicator of immune and inflammatory responses. MCP-1 regulates the activation of monocytes and macrophages with monocytes/macrophages as the main source of MCP-1.[57] IL-6 is a well-recognized pro-inflammatory cytokine, contributing to the recruitment of neutrophils, monocytes and T cells and differentiation of monocytes to macrophages.[58] IL-1β is another important pro-inflammatory cytokine affecting the pathway of the inflammatory reaction.[59] MCP-1 expression of grafts was roughly in accordance with the trend of macrophages infiltrated. LhCG showed the highest MCP-1 expression on day 1 post-implantation, followed by PC and then dLhCG. MCP-1 was expressed in BCD-LhCG whose signal was weak but still slightly visible on agarose gel. By contrast, MCP-1 expression was negligible in BCD-dLhCG and RE. 14 days later, LhCG and dLhCG, similar to PC, showed much higher MCP-1 expression compared to that of BCD-LhCG, BCD-dLhCG and RE. Moreover, it is reported that MCP-1 was secreted

mainly by pro-inflammatory M1 macrophages instead of anti-inflammatory M2 macrophages,[53] indicating that the gene expression value of MCP-1 could to some extent reflect M1 macrophage infiltration conditions. According to results in Fig. 7a and e, LhCG showed high M1 macrophage recruitment on both day 1 and day 14 which were even higher than those of positive control PC. M1 macrophage infiltration in dLhCG became more severe on day 14 compared to day 1. There were M1 macrophages infiltrated in the BCD-LhCG graft on day 1 but a reduced level was observed after 14 days. For BCD-dLhCG and negative control RE, M1 macrophages remained low in recruitment on both day 1 and day 14 based on MCP-1 expression. Furthermore, PC, dLhCG and LhCG showed a high expression value in genes encoding other two pro-inflammatory cytokines IL-6 and IL-1β on both day 1 and day 14 post-implantation. However, the expression of genes encoding pro-inflammatory cytokines was reduced or even undetectable after coating xenografts with BCD, which was comparative to the results of negative control RE and indicated that BCD could work for immune evasion. However, it is worth noting that MCP-1 expression on day 1 post-implantation and IL-1β expression on day 14 post-implantation in BCD-LhCG were reduced compared to LhCG but still detectable, implying that slight immune and inflammatory responses were induced due to the exposed antigens on the porcine ECM possibly caused by the uneven coverage of BCD on LhCG.

5. Conclusions

In this study, a novel and facile method for immune evasion of xenografts was developed by coating non-sticky albumin. The immune evasion potential of albumin was extended to the tissue engineering field. First of all, albumin was successfully modified by dopamine *via* EDC/NHS coupling for the enhancement of adhesion on grafts. LhCG and dLhCG fabricated based on our previous published protocol were chosen as the xenograft models. Dopamine modified albumin (BCD) was uniformly coated onto the surface of dLhCG, while BCD was more inclined to adhere to the cell membrane compared to the ECM in LhCG according to fluorescence images. The increase in sulphur of BCD-LhCG and BCD-dLhCG compared to LhCG and dLhCG respectively further confirmed the successful coating of BCD on the grafts. Moreover, BCD coating remained stable on both LhCG and dLhCG for at least 21 days, despite a decrease on day 7 compared to day 1. Acute immune and inflammatory responses were evaluated at cell, protein and gene levels by pathological assessment, IHC staining and PCR, respectively. LhCG showed the most serious inflammation, followed by dLhCG. However, BCD coating was proved to effectively attenuate immune and inflammatory responses with significantly reduced inflammatory cells infiltrated and lower gene expression encoding inflammation related cytokines. Slight immune and inflammatory responses were observed in BCD-LhCG due to the possible exposed antigens on the ECM, while inflammation was negligible in BCD-dLhCG. In summary, albumin coating works for alleviation of acute immune and inflammatory responses induced by LhCG and dLhCG, which could be further applied to other xenografts. In the long run, future investigations will focus on regeneration of stabilized albumin coated engineered xenografts.

Conflicts of interest

There are no conflicts to declare.

Acknowledgements

We acknowledge the funding support from the Shenzhen-Hong Kong Innovation Circle Category D Project (SGDX2019081623180779 to Dong-An Wang), Shenzhen Science and Technology Innovation Commission, China, the National Natural Science Foundation of China (NSFC51973180), the Grant AcRF Tier 2 Academic Research Fund (MOE2016-T2-1-138 (S) to Dong-An Wang), the Ministry of Education (MOE), Singapore, and, Grants from the City University of Hong Kong (9380099, 9240013, 9680269, 9678192 and 7005212).

References

1 H. Auchincloss and D. H. Sachs, *Annu. Rev. Immunol.*, 1998, **16**, 433–470.
2 E. A. Makris, A. H. Gomoll, K. N. Malizos, J. C. Hu and K. A. Athanasiou, *Nat. Rev. Rheumatol.*, 2015, **11**, 21–34.
3 S. Camarero-Espinosa, B. Rothen-Rutishauser, E. J. Foster and C. Weder, *Biomater. Sci.*, 2016, **4**, 734–767.
4 M. Cascalho and J. L. Platt, *Immunity*, 2001, **14**, 437–446.
5 H. J. Choi, J. J. Lee, M. K. Kim, H. J. Lee, A. Y. Ko, H. J. Kang, C.-G. Park and W. R. Wee, *Xenotransplantation*, 2014, **21**, 115–123.
6 V. S. De Stefano and W. J. Dupps, *Int. Ophthalmol. Clin.*, 2017, **57**, 75–86.
7 K. V. Gates, A. J. Dalgliesh and L. G. Griffiths, *Sci. Rep.*, 2017, **7**, 2446.
8 T. Parvathy, N. Divakaran, R. Lalithakunjamma, N. Vijayan, V. Syam and R. Umashankar, *Artif. Organs*, 2013, **37**, 600–605.
9 Y. S. Kim, M. Majid, A. J. Melchiorri and A. G. Mikos, *Bioeng. Transl. Med.*, 2019, **4**, 83–95.
10 T. Hoshiba, H. Lu, N. Kawazoe and G. Chen, *Expert Opin. Biol. Ther.*, 2010, **10**, 1717–1728.
11 M. C. Zhang, X. Liu, Y. Jin, D. L. Jiang, X. S. Wei and H. T. Xie, *Am. J. Transplant.*, 2015, **15**, 1068–1075.
12 U. Galili, *Biochimie*, 2001, **83**, 557–563.
13 K. R. Stone, A. Walgenbach and U. Galili, *Tissue Eng., Part B*, 2017, **23**, 412–419.
14 A. Thomas, W. J. Hawthorne and C. Burlak, *Xenotransplantation*, 2020, **27**, 1–6.
15 A. J. Dalgliesh, M. Parvizi, M. Lopera-Higuita, J. Shklover and L. G. Griffiths, *Acta Biomater.*, 2018, **79**, 253–264.
16 M. L. Wong, J. L. Wong, N. Vapniarsky and L. G. Griffiths, *Biomaterials*, 2016, **92**, 1–12.

17 F. Kratz, *J. Controlled Release*, 2014, **190**, 331–336.
18 X. M. He and D. C. Carter, *Nature*, 1992, **358**, 209–215.
19 C. Tao, Y. J. Chuah, C. Xu and D. A. Wang, *J. Mater. Chem. B*, 2019, **7**, 357–367.
20 J. R. Keogh, F. F. Velander and J. W. Eaton, *J. Biomed. Mater. Res.*, 1992, **26**, 441–456.
21 J. R. Keogh and J. W. Eaton, *J. Lab. Clin. Med.*, 1994, **124**, 537–545.
22 J. H. Park, J. A. Jackman, A. R. Ferhan, G. J. Ma, B. K. Yoon and N.-J. Cho, *ACS Appl. Mater. Interfaces*, 2018, **10**, 32047–32057.
23 I. C. Gonçalves, M. C. L. Martins, J. N. Barbosa, P. Oliveira, M. A. Barbosa and B. D. Ratner, *J. Mater. Sci.: Mater. Med.*, 2011, **22**, 2053–2063.
24 A. S. Pitek, S. A. Jameson, F. A. Veliz, S. Shukla and N. F. Steinmetz, *Biomaterials*, 2016, **89**, 89–97.
25 K. J. Koudelka, A. S. Pitek, M. Manchester and N. F. Steinmetz, *Annu. Rev. Virol.*, 2015, **2**, 379–401.
26 N. M. Gulati, A. S. Pitek, A. E. Czapar, P. L. Stewart and N. F. Steinmetz, *J. Mater. Chem. B*, 2018, **6**, 2204–2216.
27 H. Auvinen, H. Zhang, Nonappa, A. Kopilow, E. H. Niemelä, S. Nummelin, A. Correia, H. A. Santos, V. Linko and M. A. Kostiainen, *Adv. Healthcare Mater.*, 2017, **6**, 1700692.
28 Z. Li, D. Li, Q. Li, C. Luo, J. Li, L. Kou, D. Zhang, H. Zhang, S. Zhao, Q. Kan, J. Liu, P. Zhang, X. Liu, Y. Sun, Y. Wang, Z. He and J. Sun, *Biomater. Sci.*, 2018, **6**, 2681–2693.
29 B. Xia, W. Zhang, J. Shi and S. Xiao, *ACS Appl. Mater. Interfaces*, 2013, **5**, 11718–11724.
30 H. Sato, E. Nakhaei, T. Kawano, M. Murata, A. Kishimura, T. Mori and Y. Katayama, *Langmuir*, 2018, **34**, 2324–2331.
31 Y. Okamoto, K. Taguchi, K. Yamasaki, M. Sakuragi, S. Kuroda and M. Otagiri, *J. Pharm. Sci.*, 2018, **107**, 436–445.
32 H. Sato, Y. Nakamura, E. Nakhaei, D. Funamoto, C. W. Kim, T. Yamamoto, A. Kishimura, T. Mori and Y. Katayama, *Chem. Lett.*, 2014, **43**, 1481–1483.
33 B. J. Boyd, A. Galle, M. Daglas, J. V. Rosenfeld and R. Medcalf, *J. Drug Targeting*, 2015, **23**, 847–853.
34 B. P. Lee, P. B. Messersmith, J. N. Israelachvili and J. H. Waite, *Annu. Rev. Mater. Res.*, 2011, **41**, 99–132.
35 Y. Gong, K. Su, T. T. Lau, R. Zhou and D. A. Wang, *Tissue Eng., Part A*, 2010, **16**, 3611–3622.
36 W. Leong, T. T. Lau and D. A. Wang, *Acta Biomater.*, 2013, **9**, 6459–6467.
37 K. Su, T. T. Lau, W. Leong, Y. Gong and D. A. Wang, *Adv. Funct. Mater.*, 2012, **22**, 972–978.
38 Y. Peck, P. He, G. S. V. N. Chilla, C. L. Poh and D. A. Wang, *Sci. Rep.*, 2015, **5**, 16225.
39 X. Nie and D. Wang, *Biomater. Sci.*, 2018, **6**, 2798–2811.
40 X. Nie, Y. J. Chuah, W. Zhu, P. He, Y. Peck and D. A. Wang, *Biomaterials*, 2020, **235**, 119821.
41 X. Nie, J. Yang, Y. J. Chuah, W. Zhu, Y. Peck, P. He and D. A. Wang, *Adv. Healthcare Mater.*, 2020, **9**, 1901304.
42 L. Chen, H. Deng, H. Cui, J. Fang, Z. Zuo, J. Deng, Y. Li, X. Wang and L. Zhao, *Oncotarget*, 2018, **9**, 7204–7218.
43 J. M. Morais, F. Papadimitrakopoulos and D. J. Burgess, *AAPS J.*, 2010, **12**, 188–196.
44 W. Zhu, Y. Peck, J. Iqbal and D. A. Wang, *Biomaterials*, 2017, **147**, 99–115.
45 N. Barbero, L. Napione, P. Quagliotto, S. Pavan, C. Barolo, E. Barni, F. Bussolino and G. Viscardi, *Dyes Pigm.*, 2009, **83**, 225–229.
46 S. C. Gill and P. H. von Hippel, *Anal. Biochem.*, 1989, **182**, 319–326.
47 A. Papalamprou, C. W. Chang, N. Vapniarsky, A. Clark, N. Walker and L. G. Griffiths, *Acta Biomater.*, 2016, **45**, 155–168.
48 A. Dalu, B. S. Blaydes, L. G. Lomax and K. B. Delclos, *Biomaterials*, 2000, **21**, 1947–1957.
49 J. Li, A. D. Celiz, J. Yang, Q. Yang, I. Wamala, W. Whyte, B. R. Seo, N. V. Vasilyev, J. J. Vlassak, Z. Suo and D. J. Mooney, *Science*, 2017, **357**, 378–381.
50 J. Li, M. K. L. Chu, C. R. Gordijo, A. Z. Abbasi, K. Chen, H. A. Adissu, M. Löhn, A. Giacca, O. Plettenburg and X. Y. Wu, *Biomaterials*, 2015, **47**, 51–61.
51 P. Li and G. Wu, *Amino Acids*, 2018, **50**, 29–38.
52 A. O. Elzoghby, W. M. Samy and N. A. Elgindy, *J. Controlled Release*, 2012, **157**, 168–182.
53 J. Sapudom, W. K. E. Mohamed, A. Garcia-Sabaté, A. Alatoom, S. Karaman, N. Mahtani and J. C. M. Teo, *Bioengineering*, 2020, **7**, 33.
54 R. Sridharan, B. Cavanagh, A. R. Cameron, D. J. Kelly and F. J. O'Brien, *Acta Biomater.*, 2019, **89**, 47–59.
55 C. Nathan, *Nat. Rev. Immunol.*, 2006, **6**, 173–182.
56 N. Fujiwara and K. Kobayashi, *Curr. Drug Targets: Inflammation Allergy*, 2005, **4**, 281–286.
57 S. L. Deshmane, S. Kremlev, S. Amini and B. E. Sawaya, *J. Interferon Cytokine Res.*, 2009, **29**, 313–326.
58 J. Scheller, A. Chalaris, D. Schmidt-Arras and S. Rose-John, *Biochim. Biophys. Acta, Mol. Cell Res.*, 2011, **1813**, 878–888.
59 J. Hernandez-Rodriguez, *Rheumatology*, 2003, **43**, 294–301.

